Micro-Station - Modal Analysis

Dehaeze Thomas

October 24, 2024

Contents

In order to further improve the accuracy of the performance predictions, a model that better represents the micro-station dynamics is required. A multi-body model, consisting of several rigid bodies connected by kinematic constraints (i.e. joints), springs and damper elements, is a good candidate to model the micro-station.

Even though the inertia of each solid body can easily be estimated from its geometry and its material density, it is more difficult to properly estimate the stiffness and damping properties of the guiding elements connecting each solid body. The experimental modal analysis will be use to tune the model, and to verify that a multi-body model can represent accurately the dynamics of the micro-station.

The approach of tuning the multi-body model from measurements is illustrated in Figure 1. First, a *response model* is obtained, which corresponds to a set of frequency response functions computed from experimental measurements. From this response model, and modal model can be computed, which consists of two matrices: one containing the natural frequencies and damping factors of the considered modes, and another one describing the mode shapes. This modal model can then be used to tune the spatial model (i.e. the multi-body model), that is to say to tune the mass of the considering solid bodies, and the springs and dampers connecting the solid bodies.

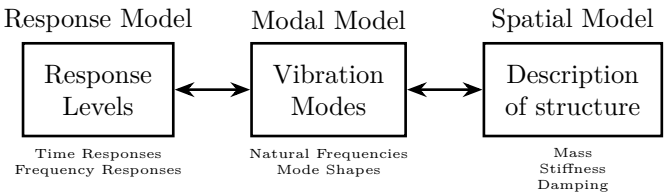

Figure 1: Figure caption

The measurement setup used to obtain the response model is presented in Section 1. This includes the instrumentation used (i.e. instrumented hammer, accelerometers and acquisition system), the test planing, and a first analysis of the obtained signals.

In Section 2, the obtained frequency response functions between the forces applied using the instrumented hammer and the various accelerometers fixed to the structure are computed. These measurements are projected at the center of mass of each considered solid body to ease the further use of the results. The solid body assumption is then verified, validating the use of the multi-body model.

Finally, the modal analysis is performed in Section 3. It shows how complex the micro-station dynamics is, and the necessity of the developed more complex multi-body model.

1 Measurement Setup

In order to perform an experimental modal analysis, a proper measurement setup is key. This include using appropriate instrumentation (presented in Section 1.1) and properly preparing the structure to be measured (Section 1.2). Then, the location of the measured motion (Section 1.3) and the location of the hammer impacts (Section 1.4) have to be chosen carefully. Obtained force and acceleration signals are shown in Section 1.5, and the quality of the measured data is checked.

1.1 Used Instrumentation

Three equipment are key to perform a good modal analysis. First, *accelerometers* are used to measure the response of the structure. Here, 3-axis accelerometers[1] shown in figure 1.1a are used. These accelerometers are glued to the micro-station using a thin layer of wax for best results **ewins00˙modal**.

(a) 3-axis accelerometer

(b) Instrumented hammer

(c) OROS acquisition system

Figure 1.1: Instrumentation used for the modal analysis

Then, an *instrumented hammer*[2] (figure 1.1b) is used to apply forces to the structure in a controlled way. Tests have been conducted to determine the most suitable hammer tip (ranging from a metallic one to a soft plastic one). The softer tip has been found to give best results as it injects more energy in the low frequency range where the coherence was low, such that the overall coherence was improved.

Finally, an *acquisition system*[3] (figure 1.1c) is used to acquire the injected force and the response accelerations in a synchronized way and with sufficiently low noise.

[1] PCB 356B18. Sensitivity is $1\,V/g$, measurement range is $\pm 5\,g$ and bandwidth is 0.5 to 5 kHz.
[2] Kistler 9722A2000. Sensitivity of $2.3\,mV/N$ and measurement range of $2\,kN$
[3] OROS OR36. 24bits signal-delta ADC.

1.2 Structure Preparation and Test Planing

In order to obtain meaningful results, the modal analysis of the micro-station in performed *in-situ*. To do so, all the micro-station stage controllers are turned "ON". This is especially important for stages for which the stiffness is provided by local feedback control, which is case for the air bearing spindle, and the translation stage. If these local feedback control were turned OFF, this would have resulted in very low frequency modes difficult to measure in practice, and this would also have lead to decoupled dynamics which would not be the case in practice.

The top part representing the active stabilization stage has been disassembled as the active stabilization stage and the sample will be added in the multi-body model afterwards.

To perform the modal-analysis from the measured responses, the $n \times n$ frequency response function matrix $\mathbf{H}$ needs to be measured, where n is the considered number of degrees of freedom. The H_{jk} element of this Frequency Response Function (FRF) matrix corresponds to the frequency response function from a force F_k applied at Degree of freedom (DoF) k to the displacement of the structure X_j at DoF j. Measuring this FRF matrix is very time consuming as it requires to make n^2 measurements. However thanks to the principle of reciprocity ($H_{jk} = H_{kj}$) and using the *point measurement* (H_{jj}), it is possible to reconstruct the full matrix by measuring only one column or one line of the matrix $\mathbf{H}$ **ewins00˙modal**. Therefore, a minimum set of n frequency response functions needs to be measured. This can be done either by measuring the response X_j at a fixed DoF j while applying forces F_i for at all n considered DoF, or by applying a force F_k at a fixed DoF k and measuring the response X_i for all n DoF.

It is however not advised to measure only one row or one column as one or more modes may be missed by an unfortunate choice of force or acceleration measured locations (for instance if the force is applied at a vibration node of a particular mode). In this modal-analysis, it is chosen to measure the response of the structure at all considered DoF, and to excite the structure at one location in three directions in order to have some redundancy and to make sure that all modes are properly energized.

1.3 Location of the Accelerometers

The location of the accelerometers fixed to the micro-station is essential as it defines where the dynamics is measured. A total of 23 accelerometers are fixed to the six key stages of the micro station: the lower and upper granites, the translation stage, the tilt stage, the spindle and the micro hexapod. The position of the accelerometers are visually shown on a CAD model in Figure 1.2 and their precise locations with respect to a frame located at the point of interest are summarized in Table 1.1. Pictures of the accelerometers fixed to the translation stage and to the micro-hexapod are shown in Figure 1.3.

As all key stages of the micro-station are foreseen to behave as solid bodies, only 6 DoF can be considered per solid body. However, it was chosen to use four 3-axis accelerometers (i.e. 12 measured DoF) for each considered solid body to have some redundancy and to be able to verify the solid body assumption (see Section 2.3).

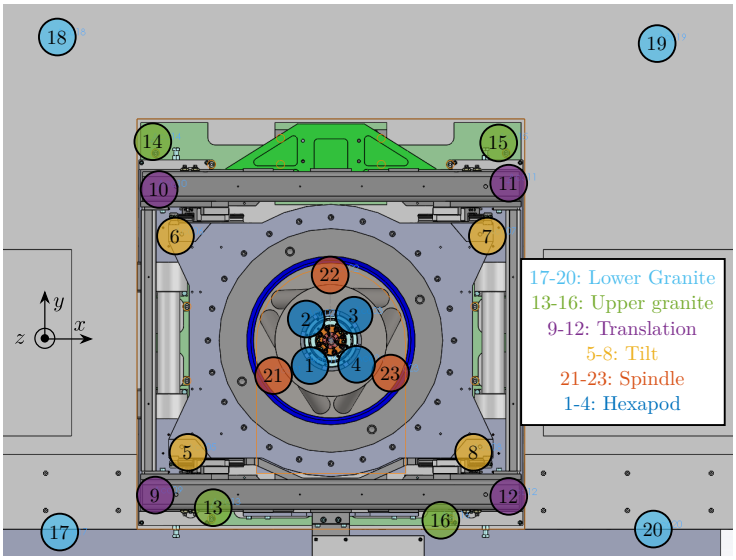

Figure 1.2: Position of the accelerometers using SolidWorks in mm

Table 1.1: Accelerometer positions

	x	y	z
Low. Granite	-730	-526	-951
Low. Granite	-735	814	-951
Low. Granite	875	799	-951
Low. Granite	865	-506	-951
Up. Granite	-320	-446	-786
Up. Granite	-480	534	-786
Up. Granite	450	534	-786
Up. Granite	295	-481	-786
Translation	-475	-414	-427
Translation	-465	407	-427
Translation	475	424	-427
Translation	475	-419	-427
Tilt	-385	-300	-417
Tilt	-420	280	-417
Tilt	420	280	-417
Tilt	380	-300	-417
Spindle	-155	-90	-594
Spindle	0	180	-594
Spindle	155	-90	-594
Hexapod	-64	-64	-270
Hexapod	-64	64	-270
Hexapod	64	64	-270
Hexapod	64	-64	-270

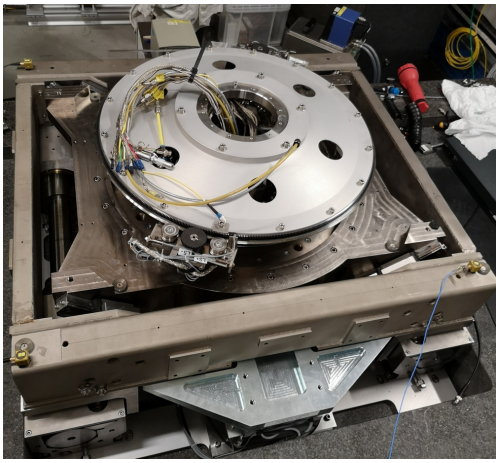

(a) T_y stage

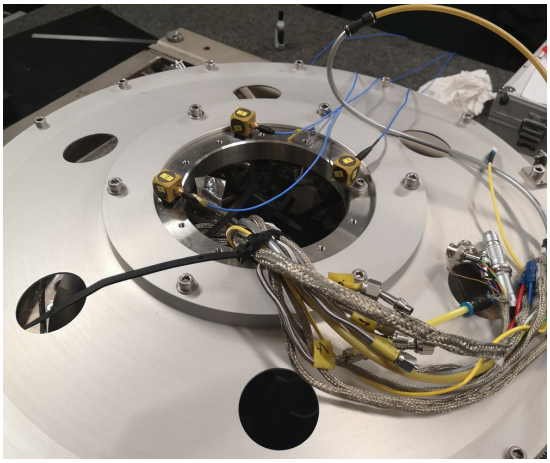

(b) Micro-Hexapod

Figure 1.3: Accelerometers fixed on the micro-station stages

1.4 Hammer Impacts

The chosen location of the hammer impact corresponds to the location of accelerometer number 11 fixed to the translation stage. It was chosen to match the location of one accelerometer, because a *point measurement* (i.e. a measurement of H_{kk}) is necessary to be able to reconstruct the full FRF matrix **ewins00˙modal**.

The impacts are performed in three directions, which are shown in figures 1.4a, 1.4b and 1.4c. This excitation point with the three considered directions allows to properly energize all the modes in the frequency band of interest and to provide good coherence for all the accelerometers as will be shown in the next section.

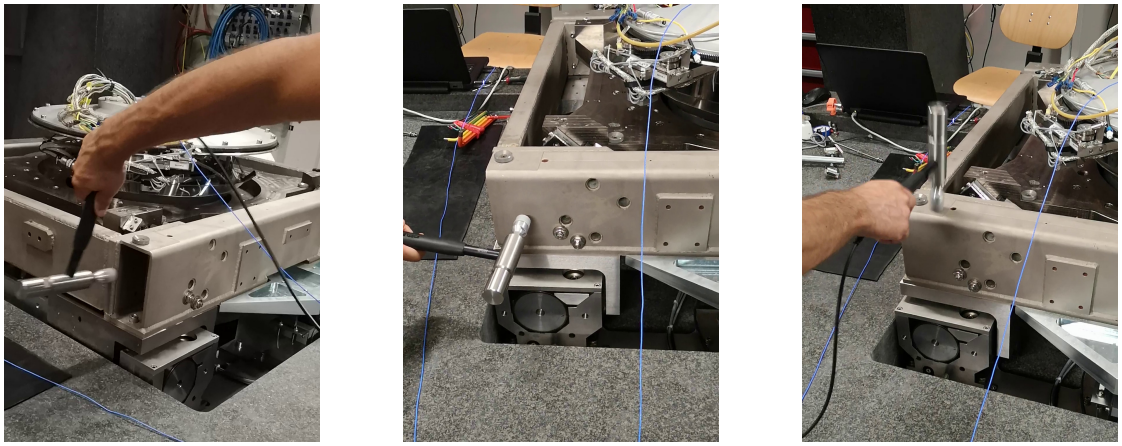

(a) X impact **(b)** Y impact **(c)** Z impact

Figure 1.4: The three hammer impacts used for the modal analysis

1.5 Force and Response signals

The force sensor of the instrumented hammer and the accelerometers signals are shown in the time domain in Figure 1.5a. Sharp "impacts" can be seen for the force sensor, indicating wide frequency band excitation. For the accelerometer, a much more complex signal can be observed, indicating complex dynamics.

The "normalized" Amplitude Spectral Density (ASD) of the two signals are computed and shown in Figure 1.5b. Conclusions based on the time domain signals can be clearly seen in the frequency domain (wide frequency content for the force signal and complex dynamics for the accelerometer).

The frequency response function H_{jk} from the applied force F_k to the measured acceleration X_j is then computed and shown Figure 1.6a. The quality of the obtained data can be estimated using the *coherence* function, which is shown in Figure 1.6b. Good coherence is obtained from 20 Hz to 200 Hz which corresponds to the frequency range of interest.

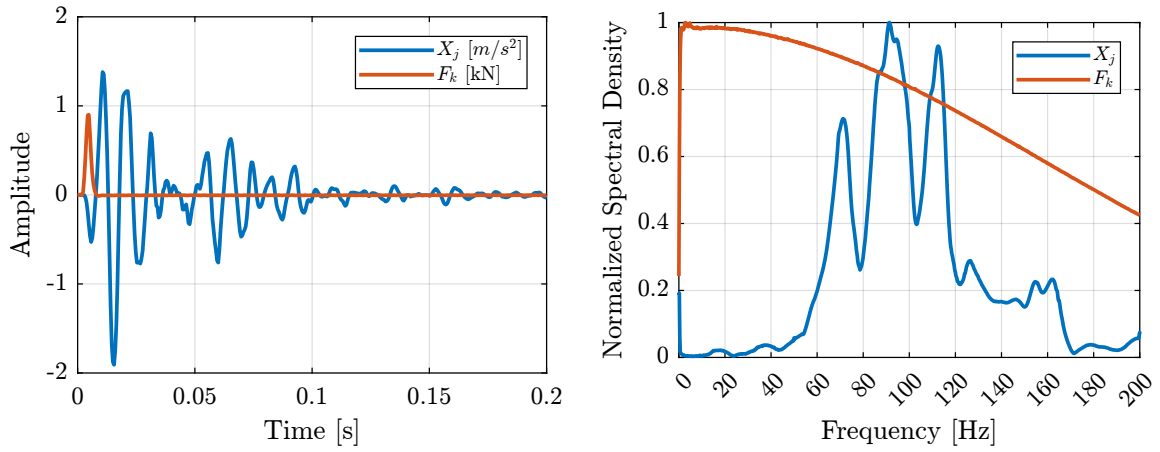

(a) Time domain signals

(b) Amplitude Spectral Density (normalized)

Figure 1.5: Raw measurement of the acceleromter (blue) and of the force sensor at the Hammer tip (red) (a). Computed Amplitude Spectral Density of the two signals (normalized) (b)

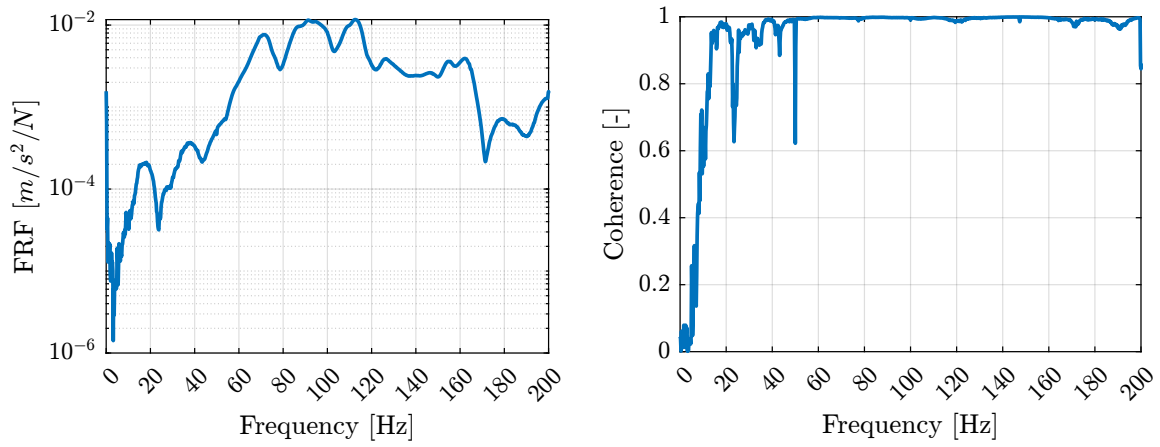

(a) Frequency Response Function

(b) Coherence

Figure 1.6: Computed frequency response function from the applied force F_k and the measured response X_j (a) as well as computed coherence (b)

2 Frequency Analysis

All measurements where conducted and a $n \times p \times q$ Frequency Response Functions Matrix were computed with:

- $n = 69$: the number of output measured accelerations (23 3-axis accelerometers)
- $p = 3$: the number of input force excitations
- $q = 801$: the number of frequency points ω_i

For each frequency point ω_i, a 2D complex matrix is obtained that links the 3 force inputs to the 69 output accelerations (2.1).

$$\mathbf{H}(\omega_i) = \begin{bmatrix} \frac{D_{1_x}}{F_x}(\omega_i) & \frac{D_{1_x}}{F_y}(\omega_i) & \frac{D_{1_x}}{F_z}(\omega_i) \\ \frac{D_{1_y}}{F_x}(\omega_i) & \frac{D_{1_y}}{F_y}(\omega_i) & \frac{D_{1_y}}{F_z}(\omega_i) \\ \frac{D_{1_z}}{F_x}(\omega_i) & \frac{D_{1_z}}{F_y}(\omega_i) & \frac{D_{1_z}}{F_z}(\omega_i) \\ \frac{D_{2_x}}{F_x}(\omega_i) & \frac{D_{2_x}}{F_y}(\omega_i) & \frac{D_{2_x}}{F_z}(\omega_i) \\ \vdots & \vdots & \vdots \\ \frac{D_{23_z}}{F_x}(\omega_i) & \frac{D_{23_z}}{F_y}(\omega_i) & \frac{D_{23_z}}{F_z}(\omega_i) \end{bmatrix} \tag{2.1}$$

However, for the multi-body model being developed, only 6 solid bodies are considered, namely: the bottom granite, the top granite, the translation stage, the tilt stage, the spindle and the hexapod. Therefore, only $6 \times 6 = 36$ degrees of freedom are of interest. The objective in this section is therefore to process the Frequency Response Matrix to reduce the number of measured DoF from 69 to 36.

In order to be able to perform this reduction of measured DoF, the rigid body assumption first needs to be verified (Section 2.1).

The coordinate transformation from accelerometers DoF to the solid body 6 DoFs (three translations and three rotations) is performed in Section 2.2. The $69 \times 3 \times 801$ frequency response matrix is then reduced to a $36 \times 3 \times 801$ frequency response matrix where the motion of each solid body is expressed with respect to its center of mass.

To further validate this reduction of DoF and the solid body assumption, the frequency response function at the accelerometer location are synthesized from the reduced frequency response matrix and are compared with the initial measurements in Section 2.3.

2.1 First verification of the solid body assumption

In this section, it is shown that two accelerometers fixed to a *rigid body* at positions $\vec{p}_1$ and $\vec{p}_2$ such that $\vec{p}_2 = \vec{p}_1 + \alpha\vec{x}$ will measure the same acceleration in the $\vec{x}$ direction. Such situation is illustrated in Figure 2.1.

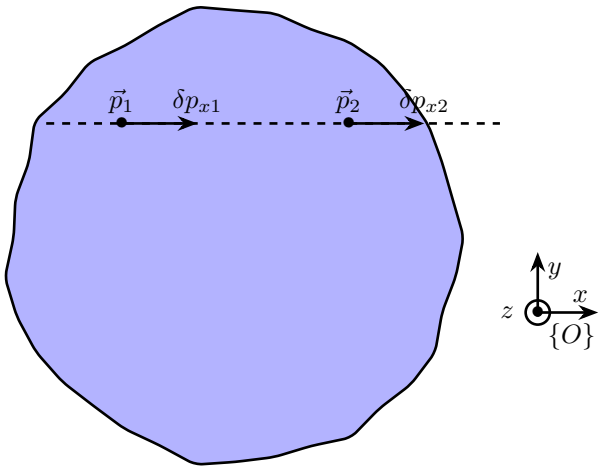

Figure 2.1: Aligned measurement of the motion of a solid body

The motion of the rigid body of figure 2.1 is here described by its displacement $\vec{\delta p} = [\delta p_x,\ \delta p_y,\ \delta p_z]$ and (small) rotations $[\delta\Omega_x,\ \delta\Omega_y,\ \delta\Omega_z]$ with respect to a reference frame $\{O\}$.

The motion of points p_1 and p_2 can be computed from $\vec{\delta p}$ and $\boldsymbol{\delta\Omega}$ (2.2), with $\boldsymbol{\delta\Omega}$ defined in (2.3).

$$\vec{\delta p}_1 = \vec{\delta p} + \boldsymbol{\delta\Omega} \cdot \vec{p}_1 \tag{2.2a}$$
$$\vec{\delta p}_2 = \vec{\delta p} + \boldsymbol{\delta\Omega} \cdot \vec{p}_2 \tag{2.2b}$$

$$\boldsymbol{\delta\Omega} = \begin{bmatrix} 0 & -\delta\Omega_z & \delta\Omega_y \\ \delta\Omega_z & 0 & -\delta\Omega_x \\ -\delta\Omega_y & \delta\Omega_x & 0 \end{bmatrix} \tag{2.3}$$

Considering only the x direction, equation (2.4) is obtained.

$$\delta p_{x1} = \delta p_x + \delta\Omega_y p_{z1} - \delta\Omega_z p_{y1} \tag{2.4a}$$
$$\delta p_{x2} = \delta p_x + \delta\Omega_y p_{z2} - \delta\Omega_z p_{y2} \tag{2.4b}$$

Because the two sensors are co-linearity in the x direction, $p_{1y} = p_{2y}$ and $p_{1z} = p_{2z}$, and (2.5) is obtained.

$$\boxed{\delta p_{x1} = \delta p_{x2}} \tag{2.5}$$

It is therefore concluded that two position sensors fixed to a rigid body will measure the same quantity in the direction "in line" the two sensors.

Such property can be used to verify that the considered stages are indeed behaving as rigid body in the frequency band of interest. From Table 1.1, the pairs of accelerometers that aligned in the X and Y directions can be identified. The response in the X direction of pairs of sensors aligned in the X direction are compared in Figure 2.2. A good match is observed up to 200Hz. Similar result is obtained for the Y direction. This therefore indicates that the considered bodies are behaving as solid bodes in the frequency range of interest.

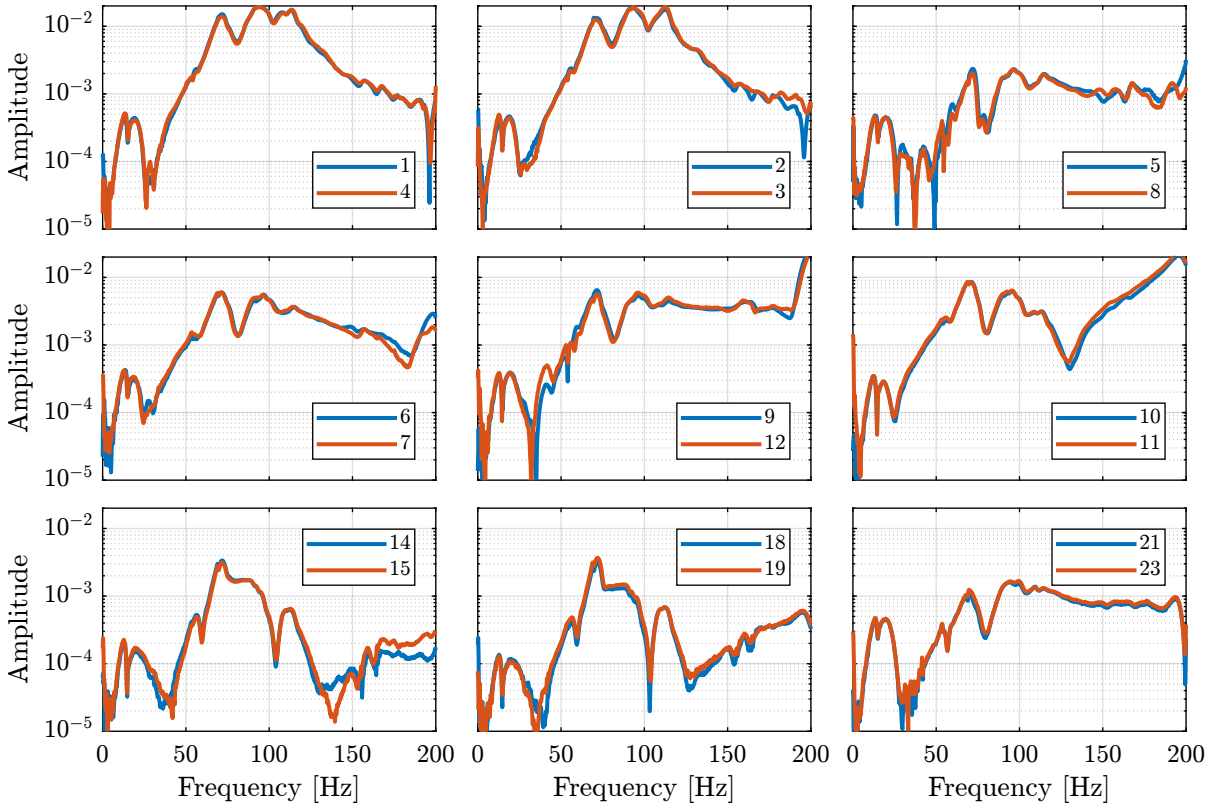

Figure 2.2: Comparaison of measured frequency response function for in the X directions for accelerometers aligned along X. Amplitude is in $\frac{m/s^2}{N}$. Accelerometer number is shown in the legend.

2.2 From accelerometer DOFs to solid body DOFs

Let's consider the schematic shown in Figure 2.3 where the motion of a solid body is measured at 4 distinct locations (in x, y and z directions). The goal here is to link these $4 \times 3 = 12$ measurements to the 6 ?? of the solid body expressed in the frame $\{O\}$.

Writing Eq. (2.2) for the four displacement sensors in a matrix form gives (2.6).

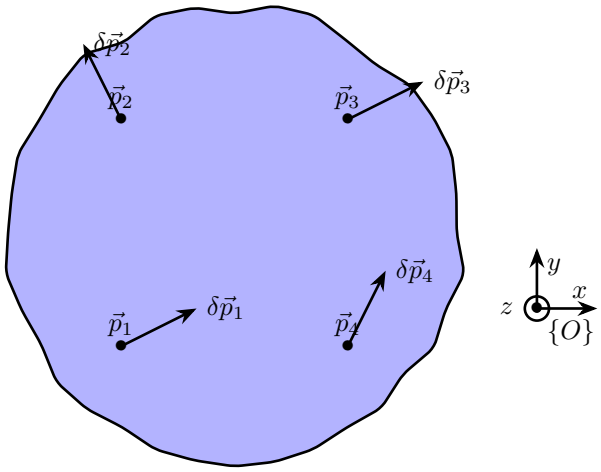

Figure 2.3: Schematic of the measured motions of a solid body

$$\left[\begin{array}{ccc|ccc} 1 & 0 & 0 & 0 & p_{1z} & -p_{1y} \\ 0 & 1 & 0 & -p_{1z} & 0 & p_{1x} \\ 0 & 0 & 1 & p_{1y} & -p_{1x} & 0 \\ \hline & \vdots & & & \vdots & \\ \hline 1 & 0 & 0 & 0 & p_{4z} & -p_{4y} \\ 0 & 1 & 0 & -p_{4z} & 0 & p_{4x} \\ 0 & 0 & 1 & p_{4y} & -p_{4x} & 0 \end{array}\right] \left[\begin{array}{c} \delta p_x \\ \delta p_y \\ \delta p_z \\ \hline \delta\Omega_x \\ \delta\Omega_y \\ \delta\Omega_z \end{array}\right] = \left[\begin{array}{c} \delta p_{1x} \\ \delta p_{1y} \\ \delta p_{1z} \\ \hline \vdots \\ \hline \delta p_{4x} \\ \delta p_{4y} \\ \delta p_{4z} \end{array}\right] \tag{2.6}$$

Supposing that the four sensors are properly located such that the system of equation (2.6) can be solved, the motion of the solid body expressed in a chosen frame $\{O\}$ using the accelerometers attached to it can be determined using equation (2.7). Note that this inversion is equivalent to resolving a mean square problem. Therefore, having more accelerometers permits to have a better approximation of the motion of the solid body.

$$\left[\begin{array}{c} \delta p_x \\ \delta p_y \\ \delta p_z \\ \hline \delta\Omega_x \\ \delta\Omega_y \\ \delta\Omega_z \end{array}\right] = \left[\begin{array}{ccc|ccc} 1 & 0 & 0 & 0 & p_{1z} & -p_{1y} \\ 0 & 1 & 0 & -p_{1z} & 0 & p_{1x} \\ 0 & 0 & 1 & p_{1y} & -p_{1x} & 0 \\ \hline & \vdots & & & \vdots & \\ \hline 1 & 0 & 0 & 0 & p_{4z} & -p_{4y} \\ 0 & 1 & 0 & -p_{4z} & 0 & p_{4x} \\ 0 & 0 & 1 & p_{4y} & -p_{4x} & 0 \end{array}\right]^{-1} \left[\begin{array}{c} \delta p_{1x} \\ \delta p_{1y} \\ \delta p_{1z} \\ \hline \vdots \\ \hline \delta p_{4x} \\ \delta p_{4y} \\ \delta p_{4z} \end{array}\right] \tag{2.7}$$

From the CAD model, the position of the center of mass of each considered solid body is computed (see Table 2.1). Then, the position of each accelerometer with respect to the center of mass of the corresponding solid body can easily be derived.

Using (2.7), the frequency response matrix $\boldsymbol{H}_{\text{CoM}}$ (2.8) expressing the response D_i (i from 1 to 6 for the 6 considered solid bodies) at the center of mass of each solid body can be computed from the initial FRF matrix $\boldsymbol{H}$.

Table 2.1: Center of mass of considered solid bodies with respect to the "point of interest"

	X [mm]	Y [mm]	Z [mm]
Bottom Granite	45	144	-1251
Top granite	52	258	-778
Translation stage	0	14	-600
Tilt Stage	0	-5	-628
Spindle	0	0	-580
Hexapod	-4	6	-319

$$\boldsymbol{H}_{\text{CoM}}(\omega_i) = \begin{bmatrix} \frac{D_{1,T_x}}{F_x}(\omega_i) & \frac{D_{1,T_x}}{F_y}(\omega_i) & \frac{D_{1,T_x}}{F_z}(\omega_i) \\ \frac{D_{1,T_y}}{F_x}(\omega_i) & \frac{D_{1,T_y}}{F_y}(\omega_i) & \frac{D_{1,T_y}}{F_z}(\omega_i) \\ \frac{D_{1,T_z}}{F_x}(\omega_i) & \frac{D_{1,T_z}}{F_y}(\omega_i) & \frac{D_{1,T_z}}{F_z}(\omega_i) \\ \frac{D_{1,R_x}}{F_x}(\omega_i) & \frac{D_{1,R_x}}{F_y}(\omega_i) & \frac{D_{1,R_x}}{F_z}(\omega_i) \\ \frac{D_{1,R_y}}{F_x}(\omega_i) & \frac{D_{1,R_y}}{F_y}(\omega_i) & \frac{D_{1,R_y}}{F_z}(\omega_i) \\ \frac{D_{1,R_z}}{F_x}(\omega_i) & \frac{D_{1,R_z}}{F_y}(\omega_i) & \frac{D_{1,R_z}}{F_z}(\omega_i) \\ \frac{D_{2,T_x}}{F_x}(\omega_i) & \frac{D_{2,T_x}}{F_y}(\omega_i) & \frac{D_{2,T_x}}{F_z}(\omega_i) \\ \vdots & \vdots & \vdots \\ \frac{D_{6,R_z}}{F_x}(\omega_i) & \frac{D_{6,R_z}}{F_y}(\omega_i) & \frac{D_{6,R_z}}{F_z}(\omega_i) \end{bmatrix} \tag{2.8}$$

2.3 Verification of solid body assumption

From the response of one solid body along its 6 ?? (from $\boldsymbol{H}_{\text{CoM}}$), and using (2.6), it is possible to compute the response of the same solid body at any location, in particular at the location of the accelerometers fixed to this solid body.

Comparing the computed response of a particular accelerometer from $\boldsymbol{H}_{\text{CoM}}$ with the original measurements $\boldsymbol{H}$ is useful to check if the change of coordinate (2.7) works as expected, and if the solid body assumption is correct in the frequency band of interest.

The comparison is made for the 4 accelerometers fixed to the micro-hexapod in Figure 2.4. The original frequency response functions and the ones computed from the CoM responses are well matching in the frequency range of interested. Similar results are obtained for the other solid bodies, indicating that the solid body assumption is valid, and that a multi-body model can be used to represent the dynamics of the micro-station. This also validates the reduction of the number of degrees of freedom from 69 (23 accelerometers with each 3acrshort:dof) to 36 (6 solid bodies with 6 DoF).

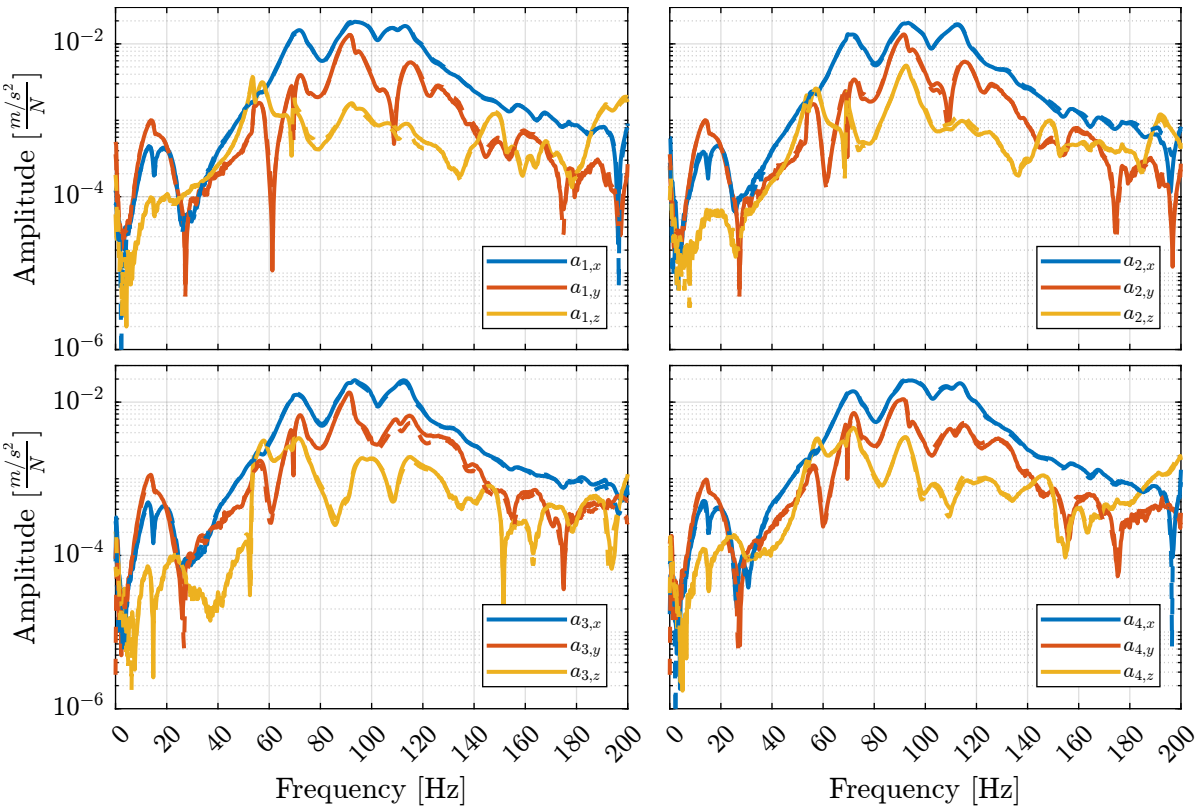

Figure 2.4: Comparaison of the original accelerometer response (solid curves) and reconstructed response from the solid body response (dashed curves). For accelerometers 1 to 4 corresponding to the micro-hexapod.

3 Modal Analysis

The goal here is to extract the modal parameters describing the modes of station being studied, namely:

- the eigen frequencies and the modal damping (eigen values)
- the mode shapes (eigen vectors)

This is done from the FRF matrix previously extracted from the measurements.

In order to do the modal parameter extraction, we first have to estimate the order of the modal model we want to obtain. This corresponds to how many modes are present in the frequency band of interest. In section 3.1, we will use the Singular Value Decomposition and the Modal Indication Function to estimate the number of modes.

The modal parameter extraction methods generally consists of **curve-fitting a theoretical expression for an individual FRF to the actual measured data**. However, there are multiple level of complexity:

- works on a part of a single FRF curve
- works on a complete curve encompassing several resonances
- works on a set of many FRF plots all obtained from the same structure

The third method is the most complex but gives better results. This is the one we will use in section 3.2.

From the modal model, it is possible to obtain a graphic display of the mode shapes (section 3.3).

In order to validate the quality of the modal model, we will synthesize the FRF matrix from the modal model and compare it with the FRF measured (section 3.4).

The modes of the structure are expected to be complex, however real modes are easier to work with when it comes to obtain a spatial model from the modal parameters.

3.1 Determine the number of modes

Singular Value Decomposition - Modal Indication Function The Mode Indicator Functions are usually used on $n \times p$ FRF matrix where n is a relatively large number of measurement DOFs and p is the number of excitation DOFs, typically 3 or 4.

In these methods, the frequency dependent FRF matrix is subjected to a singular value decomposition analysis which thus yields a small number (3 or 4) of singular values, these also being frequency dependent.

These methods are used to **determine the number of modes** present in a given frequency range, to **identify repeated natural frequencies** and to pre-process the FRF data prior to modal analysis.

From the documentation of the modal software:

> he MIF consist of the singular values of the Frequency response function matrix. The number of MIFs equals the number of excitations. By the powerful singular value decomposition, the real signal space is separated from the noise space. Therefore, the MIFs exhibit the modes effectively. A peak in the MIFs plot usually indicate the existence of a structural mode, and two peaks at the same frequency point means the existence of two repeated modes. Moreover, the magnitude of the MIFs implies the strength of the a mode.

Important

The **Complex Mode Indicator Function** is defined simply by the SVD of the FRF (sub) matrix:

$$[H(\omega)]_{n\times p} = [U(\omega)]_{n\times n}[\Sigma(\omega)]_{n\times p}[V(\omega)]^H_{p\times p}$$
$$[CMIF(\omega)]_{p\times p} = [\Sigma(\omega)]^T_{p\times n}[\Sigma(\omega)]_{n\times p}$$

We compute the Complex Mode Indicator Function. The result is shown on Figure 3.1.

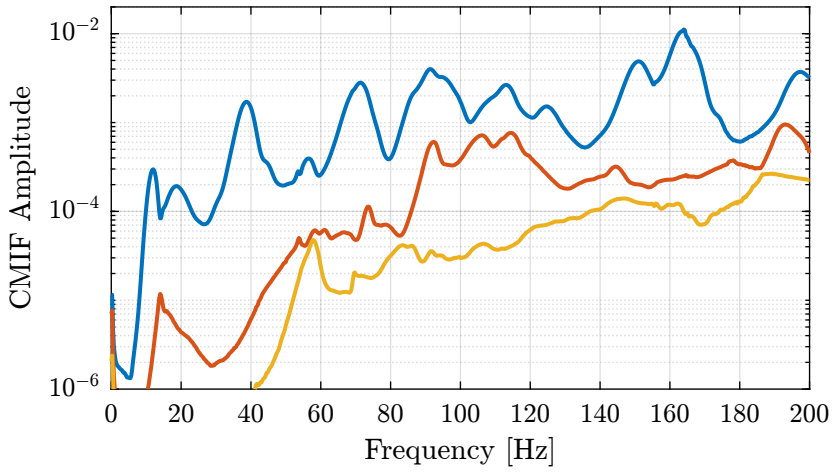

Figure 3.1: Modal Indication Function

Composite Response Function An alternative is the Composite Response Function $HH(\omega)$ defined as the sum of all the measured FRF:

$$HH(\omega) = \sum_j \sum_k H_{jk}(\omega) \tag{3.1}$$

Instead, we choose here to use the sum of the norms of the measured frf:

$$HH(\omega) = \sum_j \sum_k |H_{jk}(\omega)| \tag{3.2}$$

The result is shown on figure 3.2.

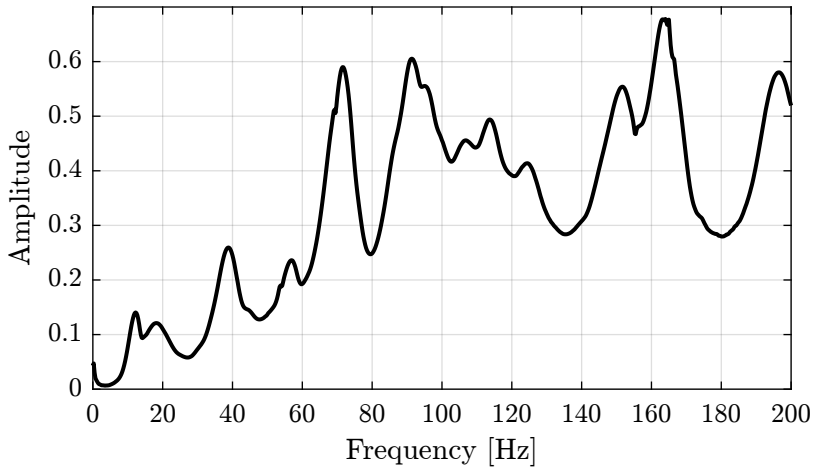

Figure 3.2: Composite Response Function

3.2 Modal parameter extraction

OROS - Modal software Modal identification are done within the Modal software of OROS.

Several modal parameter extraction methods are available. We choose to use the "broad band" method as it permits to identify the modal parameters using all the FRF curves at the same time. It takes into account the fact the the properties of all the individual curves are related by being from the same structure: all FRF plots on a given structure should indicate the same values for the natural frequencies and damping factor of each mode.

Such method also have the advantage of producing a **unique and consistent model** as direct output.

In order to apply this method, we select the frequency range of interest and we give an estimate of how many modes are present.

Then, it shows a stabilization charts, such as the one shown on figure 3.3, where we have to manually select which modes to take into account in the modal model.

We can then run the modal analysis, and the software will identify the modal damping and mode shapes at the selected frequency modes.

Importation of the modal parameters on Matlab The obtained modal parameters are:

- Resonance frequencies in Hertz

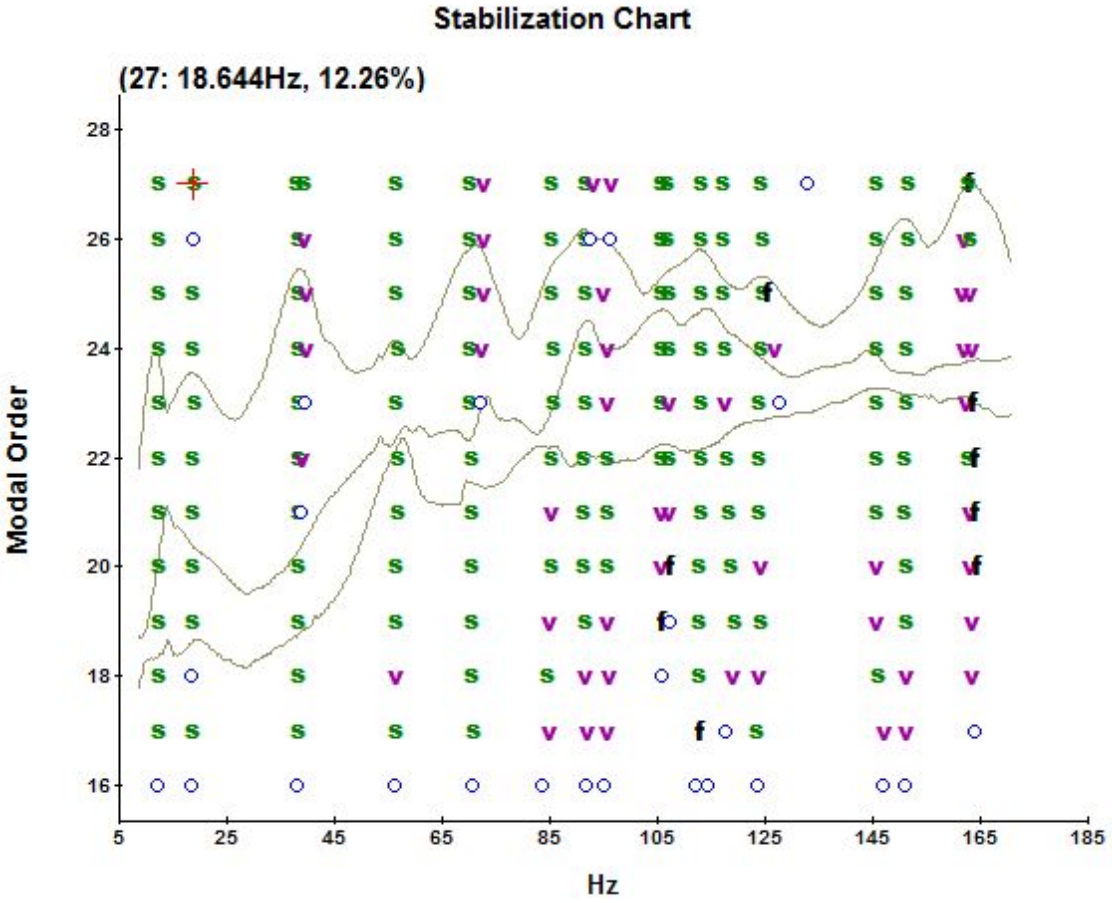

Figure 3.3: Stabilization Chart

- Modal damping ratio in percentage
- (complex) Modes shapes for each measured DoF
- Modal A and modal B which are parameters important for further normalization

The obtained mode frequencies and damping are shown in Table 3.1.

Table 3.1: Obtained eigen frequencies and modal damping

Mode	Frequency [Hz]	Damping [%]
1	11.9	12.2
2	18.6	11.7
3	37.8	6.2
4	39.1	2.8
5	56.3	2.8
6	69.8	4.3
7	72.5	1.3
8	84.8	3.7
9	91.3	2.9
10	105.5	3.2
11	106.6	1.6
12	112.7	3.1
13	124.2	2.8
14	145.3	1.3
15	150.5	2.4
16	165.4	1.4

Theory It seems that the modal analysis software makes the **assumption** of viscous damping for the model with which it tries to fit the FRF measurements.

If we note N the number of modes identified, then there are $2N$ eigenvalues and eigenvectors given by the software:

$$s_r = \omega_r(-\xi_r + i\sqrt{1-\xi_r^2}), \quad s_r^* \tag{3.3}$$

$$\{\psi_r\} = \begin{Bmatrix} \psi_{1_x} & \psi_{2_x} & \dots & \psi_{23_x} & \psi_{1_y} & \dots & \psi_{1_z} & \dots & \psi_{23_z} \end{Bmatrix}^T, \quad \{\psi_r\}^* \tag{3.4}$$

for $r = 1, \dots, N$ where ω_r is the natural frequency and ξ_r is the critical damping ratio for that mode.

Modal Matrices We would like to arrange the obtained modal parameters into two modal matrices:

$$\Lambda = \begin{bmatrix} s_1 & & 0 \\ & \ddots & \\ 0 & & s_N \end{bmatrix}_{N\times N}; \quad \Psi = \begin{bmatrix} & & \\ \{\psi_1\} & \dots & \{\psi_N\} \\ & & \end{bmatrix}_{M\times N}$$

$$\{\psi_i\} = \begin{Bmatrix} \psi_{i,1_x} & \psi_{i,1_y} & \psi_{i,1_z} & \psi_{i,2_x} & \dots & \psi_{i,23_z} \end{Bmatrix}^T$$

M is the number of DoF: here it is $23 \times 3 = 69$. N is the number of mode

Each eigen vector is normalized: $\|\{\psi_i\}\|_2 = 1$

However, the eigen values and eigen vectors appears as complex conjugates:

$$s_r, s_r^*, \{\psi\}_r, \{\psi\}_r^*, \quad r = 1, N$$

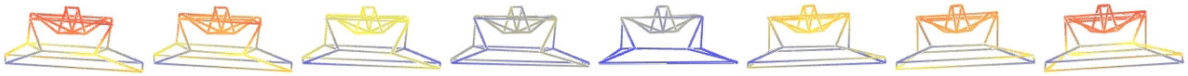

(a) Mode 1

(b) Mode 6

(c) Mode 13

Figure 3.4: Instrumentation used for the modal analysis

In the end, they are $2N$ eigen values. We then build two extended eigen matrices as follow:

$$\mathcal{S} = \begin{bmatrix} s_1 & & & & & \\ & \ddots & & & 0 & \\ & & s_N & & & \\ & & & s_1^* & & \\ & 0 & & & \ddots & \\ & & & & & s_N^* \end{bmatrix}_{2N \times 2N} \quad ; \quad \Phi = \begin{bmatrix} \{\psi_1\} & \dots & \{\psi_N\} & \{\psi_1^*\} & \dots & \{\psi_N^*\} \end{bmatrix}_{M \times 2N}$$

We also build the Modal A and Modal B matrices:

$$A = \begin{bmatrix} a_1 & & 0 \\ & \ddots & \\ 0 & & a_N \end{bmatrix}_{N \times N} \quad ; \quad B = \begin{bmatrix} b_1 & & 0 \\ & \ddots & \\ 0 & & b_N \end{bmatrix}_{N \times N} \tag{3.5}$$

With a_i is the "Modal A" parameter linked to mode i.

"Modal A" and "modal B" are linked through the following formula:

$$B = -A\Lambda$$

3.3 Obtained Mode Shapes animations

From the modal parameters, it is possible to show the modal shapes with an animation.

Examples are shown in Figures 3.4.

We can learn quite a lot from these mode shape animations.

For instance, the mode shape of the first mode at 11Hz (figure 3.4a) seems to indicate that this corresponds to a suspension mode.

This could be due to the 4 Airloc Levelers that are used for the granite (figure 3.5).

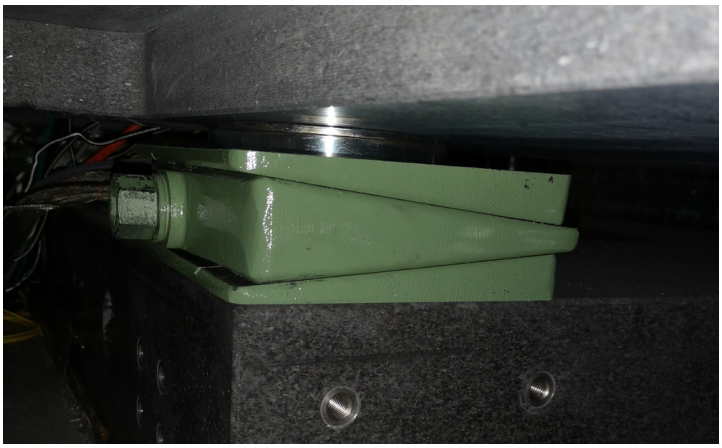

Figure 3.5: AirLoc used for the granite (2120-KSKC)

They are probably **not well leveled**, so the granite is supported only by two Airloc.

3.4 Verify the validity of the Modal Model

There are two main ways to verify the validity of the modal model

- Synthesize FRF measurements that has been used to generate the modal model and compare
- Synthesize FRF that has not yet been measured. Then measure that FRF and compare

From the modal model, we want to synthesize the Frequency Response Functions that has been used to build the modal model.

Let's recall that:

- M is the number of measured DOFs ($3 \times n_{\text{acc}}$)
- N is the number of modes identified

We then have that the FRF matrix $[H_{\text{syn}}]$ can be synthesize using the following formula:

Important

$$[H_{\text{syn}}(\omega)]_{M\times M} = [\Phi]_{M\times 2N} \left[\frac{Q_r}{j\omega - s_r}\right]_{2N\times 2N} [\Phi]^T_{2N\times M} \tag{3.6}$$

with $Q_r = 1/M_{A_r}$

An alternative formulation is:

$$H_{pq}(s_i) = \sum_{r=1}^{N} \frac{A_{pqr}}{s_i - \lambda_r} + \frac{A^*_{pqr}}{s_i - \lambda^*_r}$$

with:

- $A_{pqr} = \frac{\psi_{pr}\psi_{qr}}{M_{A_r}}$, M_{A_r} is called "Modal A"
- ψ_{pr}: scaled modal coefficient for output DOF p, mode r
- λ_r: complex modal frequency

From the modal software documentation:

> Modal A Scaling constant for a complex mode. It has the same properties as modal mass for normal modes (undamped or proportionally damped cases). Assuming
>
> - ψ_{pr} = Modal coefficient for measured degree of freedom p and mode r
> - ψ_{qr} = Modal coefficient for measured degree of freedom q and mode r
> - A_{pqr} = Residue for measured degree of freedom p, measured degree of q and mode r
> - M_{Ar} = Modal A of mode r
>
> Then
>
> $$A_{pqr} = \frac{\psi_{pr}\psi_{qr}}{M_{Ar}}$$
>
> **Modal B** Scaling constant for a complex mode. It has the same properties as modal stiffness for normal modes (undamped or proportionally damped cases). Assuming
>
> - M_{Ar} = Modal A of mode r
> - λ_r = System pole of mode r
>
> Then
>
> $$M_{Br} = -\lambda_r M_{Ar}$$

The comparison between the original measured frequency response function and the synthesized one from the modal model is done in Figure 3.6.

Frequency response functions that has not been measured can be synthesized as shown in Figure 3.7.

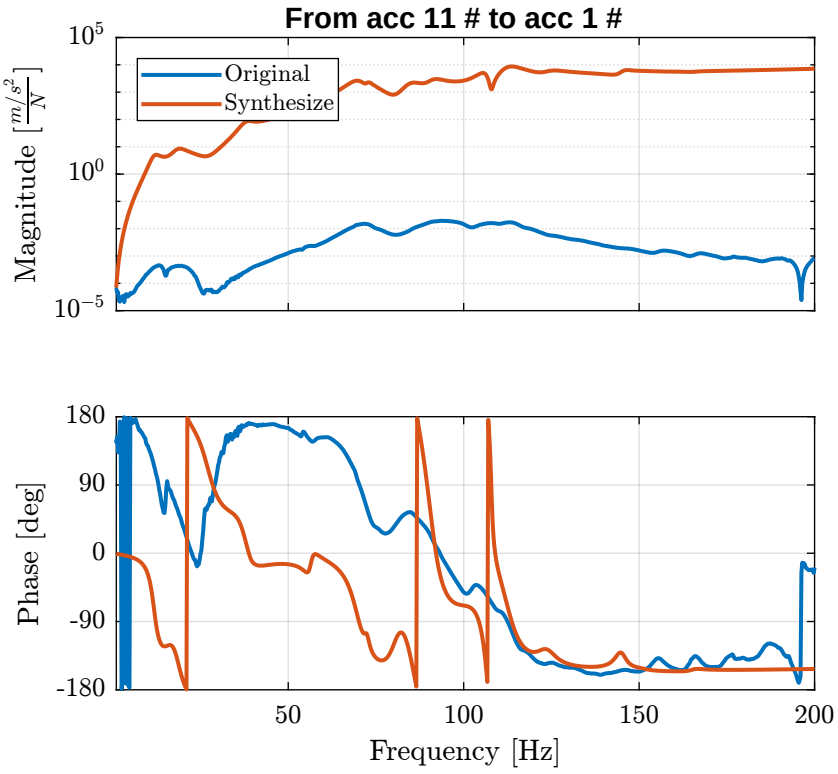

Figure 3.6: description

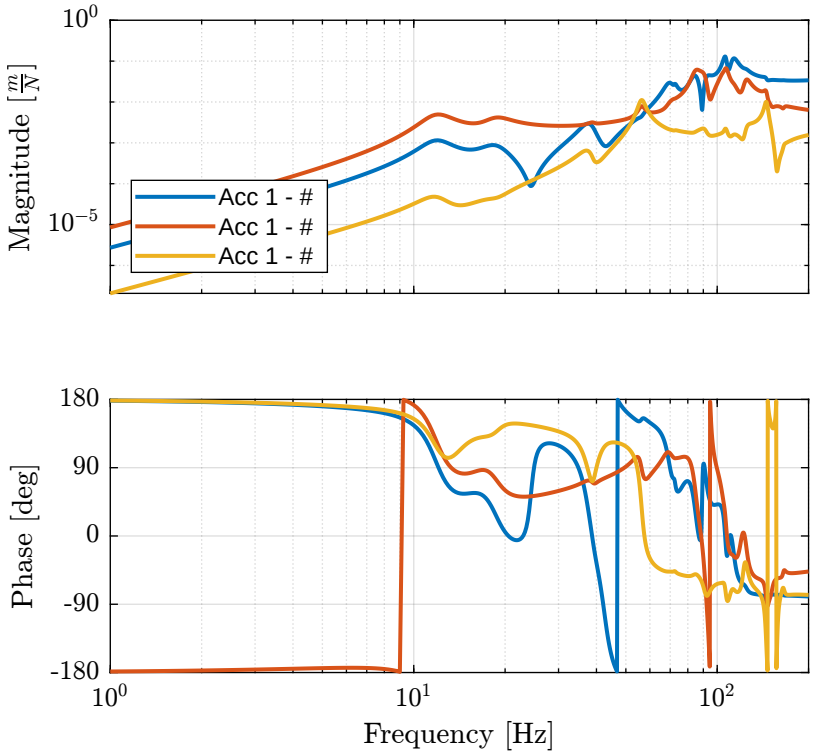

Figure 3.7: description

4 Conclusion

Validation of solid body model.

Further step: go from modal model to parameters of the solid body model.